

Broadband Light Extraction from White Organic Light-Emitting Devices by Employing Corrugated Metallic Electrodes with Dual Periodicity

Yan-Gang Bi, Jing Feng,* Yun-Fei Li, Xu-Lin Zhang, Yue-Feng Liu, Yu Jin, and Hong-Bo Sun*

White organic light-emitting diodes (WOLEDs) are of interest on the grounds of their potential applications for full-color flat-panel displays and solid-state lighting.^[1,2] High efficiency is a key issue for their commercial applications, while a very low light extraction efficiency of less than 20 % is a stumbling block for this high efficiency. More than 80 % photons produced by exciton decay are trapped inside OLEDs in the form of waveguide (WG) modes in organic/indium–tin oxide (ITO) anode layers, surface plasmon–polariton (SPP) modes associated with the metallic electrode/organic interface, and substrate modes from total internal reflection at the glass substrate/air interface.^[3–5] These trapped photons represent the area in which there is still the greatest scope for significant improvements in efficiency through an efficient recovery of the lost power. Broadband extraction is important for the efficient outcoupling of the trapped photons, especially for those trapped in WOLEDs whose spectra covers the whole visible wavelength. Broadband extraction of the substrate modes can easily be realized by attaching a microlens array on the outside of the substrate. However, in the case of the SPP and WG modes inside of the OLEDs, structure modification has to be introduced inside the device structure and broadband extraction is difficult to obtain. Wavelength-scale periodic microstructures introduced into the OLEDs are suitable for a specific narrow range of wavelengths as they satisfy the Bragg scattering condition, and are applicable only for monochromatic OLEDs.^[3,5–9] Other microstructures, such as spontaneously formed buckles or defective hexagonal-close-packed arrays, have been used to effectively enhance light extraction for OLEDs,^[10,11] while their effect on broadband light extraction in WOLEDs has not yet been examined. So far, broadband light extraction from WOLEDs is still a challenge for its applications in both display and lighting.

OLEDs with two metallic electrodes that employ a metallic film with high optical transmission and electrical conductivity

to replace ITO as the anode could eliminate the power lost to the WG modes in ITO.^[3,12] In this case, light trapped in the SPP modes would represent the main power lost, and therefore, highly efficient light extraction could be expected by broadband excitation and outcoupling of the SPP modes in the WOLEDs. Recently, the use of dual plasmonic nanostructures with Au nanoparticles embedded in a periodic corrugated active polymer layer by nanoimprinting has been reported to achieve broadband light absorption in organic solar cells,^[13] which might provide a possibility to excite broadband SPP modes for WOLEDs. However, nanoimprinting is usually applicable to polymer films and has limitations in small-molecule-based devices. Herein, broadband excitation and outcoupling of the SPP modes in WOLEDs has been realized by introducing a two-dimensional (2D) grating with dual-periodic corrugation into the WOLEDs. The 2D grating consists of two sets of corrugations with different periods that can broaden the SPP resonance relative to that of the monoperiodic grating. Blue and orange emission are both efficiently extracted from the WOLEDs based on two complementary color strategies by adjusting appropriate periods of the dual-periodic corrugation. Both experimental and numerical results support the validity of the broadband light extraction, and a 48 % enhancement in the external quantum efficiency compared to those of the conventional planar devices is obtained.

Figure 1a–c shows a schematic of the broadband light extraction using dual-periodic corrugation. Holographic lithography was employed to fabricate a dual-periodic corrugation on the surface of a photoresist film, which is a simple approach with high controllability and reproducibility.^[3,5] The dual-periodic corrugation has two sets of grating with different periods that are rotated 60° with respect to each other. 1D monoperiodic corrugations were also prepared by the same technology for comparison. The morphologies on the photoresist surface were investigated by atomic force microscopy (AFM), and are shown in Figure 1d–f. The groove depth was found to be about 60 nm for the periodic corrugation by tuning the laser fluence.^[9] In general, WOLEDs can be obtained by three complementary color strategies (red, green, and blue) or two complementary color strategies (orange and blue) applied in a multi- or a single-layer structure.^[14,15] Here, a simple WOLED with two color strategies was fabricated on the dual-periodic corrugated substrate based on a single emitting layer by doping bis(7,8-benzoquinolino)iridium(III) (*N,N'*-diisopropylbenzamide) [(bzq)₂Ir(dipba)], an orange-emitting phosphorescent material, into a blue-emitting fluorescent complex bis(2-(2-hydroxyphenyl)-pyridine)beryllium) (Bepp₂).^[14] The structure

Y.-G. Bi, Prof. J. Feng, Y.-F. Li, X.-L. Zhang, Y.-F. Liu,
Y. Jin, Prof. H.-B. Sun
State Key Laboratory on Integrated Optoelectronics
College of Electronic Science and Engineering
Jilin University, 2699 Qianjin Street,
Changchun, 130012, P.R. China
E-mail: jingfeng@jlu.edu.cn; hbsun@jlu.edu.cn
Prof. H.-B. Sun
College of Physics, Jilin University
119 Jiefang Road, Changchun, 130023, P.R. China



DOI: 10.1002/adma.201302367

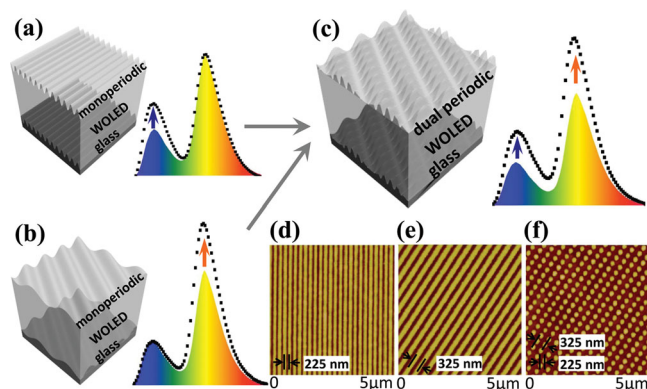


Figure 1. a–c) Schematic of the broadband light extraction by using dual-periodic corrugation. d–f) AFM images of surface morphologies of photoresist with 1D period of d) 225 and e) 325 nm, and f) 2D dual-periodic corrugation.

of the corrugated WOLED is Au (15 nm)/MoO₃ (5 nm)/NPB (40 nm)/Bepp₂:(bzq)₂Ir(dipba) (20 nm, 2 wt%)/Bepp₂ (45 nm)/LiF (1 nm)/Al (80 nm). 1D monoperiodic corrugated and planar WOLEDs with the same device structure were also fabricated for comparison.

The emission wavelengths for the two-color-based WOLEDs are around 450 and 575 nm (Figure S1, Supporting Information); these arise from the emission of the blue emitter Bepp₂ and orange emitter (bzq)₂Ir(dipba), respectively. By taking into account that the SPP resonance at the corrugated metal surface can be tuned by adjusting the grating period, the SPP resonance at the two wavelengths of 450 and 575 nm can be obtained by well-designed corrugations with favorable periods. Absorption spectra of the 1D WOLEDs with various grating periods from 225 to 350 nm were measured to determine the favorable periods (Figure S2), and the periods were determined to be 225 and 325 nm. A planar WOLED was used as the reference sample for the absorption measurement of the corrugated WOLEDs, to exclude absorption by the planar metal and organic films in the observed wavelength region, so that the peaks that originated from the SPP resonance supported by the periodic corrugation could be distinguished clearly. The thickness of the Al cathode was 50 nm according to the absorption measurement. The absorption spectra as a function of observation angles of the WOLEDs integrated with the 1D periodic corrugations with periods of 225 and 325 nm are shown in Figure 2a and b. The absorption peak in the normal direction is located at around 450 nm (Figure 2a) for the corrugated period of 225 nm, while it is 575 nm for the period of 325 nm (Figure 2b); these values are coincident with the two peak wavelengths of the two-color-based WOLEDs. The absorption peak splits into two peaks, and shifts in wavelength with the increased observation angle. The two periods of 225 and 325 nm are combined to form the dual-periodic corrugation. Figure 2c shows the absorption spectra for the dual-periodic-corrugated WOLEDs. The spectra exhibit broadband absorption and are more complex than those of the two 1D WOLEDs alone. Two peaks at 450 and 575 nm both appear in the normal direction, and they coincide with those of the two 1D corrugated devices. The angular-dependent absorption spectra have

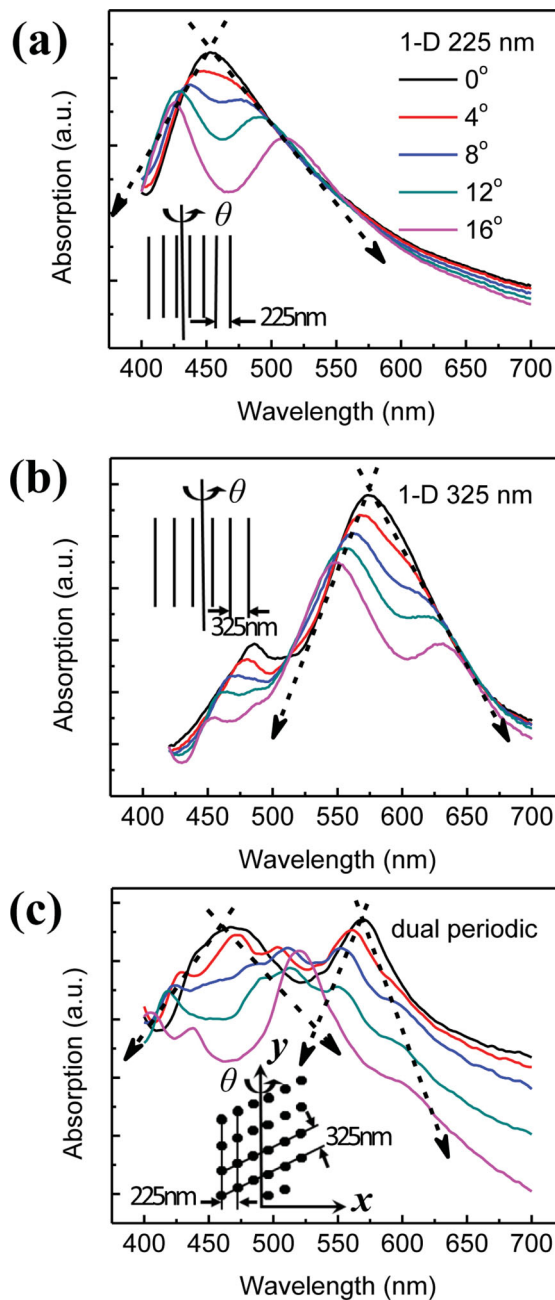


Figure 2. The angular-dependent absorption spectra for the 1D WOLEDs with a grating period of a) 225 and b) 325 nm, and c) 2D WOLEDs with the dual-periodic corrugation. The insets show the orientation of the rotation axis, which is parallel to the grooves (one of the grooves for the 2D corrugation) of the microstructure for the measurement.

been further examined by using a transverse mode (TM) and transverse-electric (TE) polarized light source (Figure S3). It can be distinguished clearly that the two peaks in the normal direction correspond to the optical modes supported by the 225- and 325-nm grating periods. We can conclude from the absorption spectrum of the dual-periodic grating is favorable for broadband light extraction because of the coincidence of the optical modes with the two emitting peaks of the two-color WOLEDs.

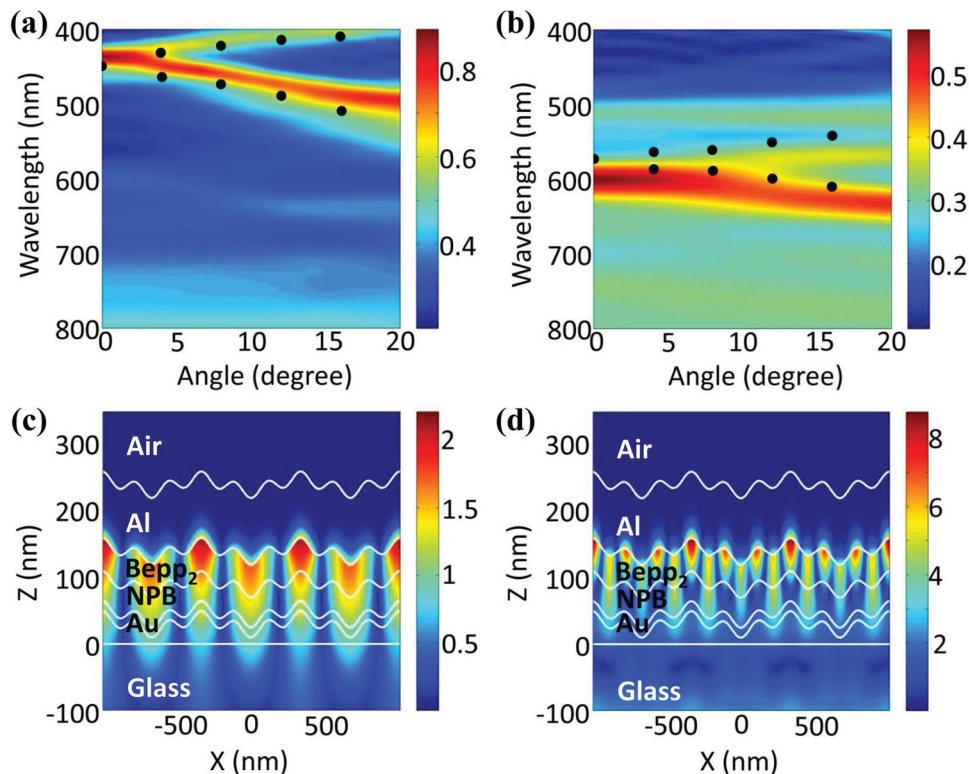


Figure 3. Calculated dispersion relations for the wavelength versus incident angles of the dual-periodic WOLEDs for a) TM and b) TE polarization, and distributions of the magnetic field intensity across the 2D WOLEDs with the normal incident light at c) 450 nm with TM polarization and d) 575 nm with TE polarization. The measured dispersion relations extracted from the absorption spectra (circles) are also shown in (a) and (b).

To establish the optical modes supported by WOLEDs with the dual-periodic corrugation, absorption spectra were simulated by using in-house-generated finite-difference time-domain (FDTD) codes.^[3,9] The two periods were approximated to be 230 and 330 nm, and a region of 660×380 nm was used as the simulated cell (Figure S4). The simulated dispersion maps with TM and TE polarized incident light are shown in Figure 3a and b, respectively, in which the absorption intensity is shown as a function of both incident angles and absorption wavelength. More specifically, the incidence with the electric and magnetic component vertical with the xz plane can be called TE and TM polarized incidence, respectively. Dispersion relations constructed from the measured absorption spectra with TM and TE polarization (Figure S3) are also plotted in Figure 3a and b. There is an excellent agreement between the numerically calculated and experimentally measured dispersion relations. To identify the optical modes supported by the corrugated WOLEDs, spatial steady-state H_z field intensity distributions across the device structure as a function of position of the normal incident light were calculated for the device with the dual-periodic corrugation. The field-intensity distributions for the TM polarization with wavelength of 450 nm and TE polarization with wavelength of 575 nm are shown in Figure 3c and d, respectively. The field intensity exhibits its maximum at the Al/organic interface and decays along the direction perpendicular to it, which demonstrates that the absorption peaks at 450 and 575 nm both originate from SPP modes, since SPPs

are surface waves and propagate along the interface between a metal and a dielectric material.^[16–19] SPP modes at the Au anode/organic interface were not observed in either experimental or numerical results, which means that they may not be supported within the wavelength range of interest. Both the dispersion relations and field distributions were calculated for the 1D WOLEDs and shown in Figure S5, which also demonstrates the excitation of the SPPs at the Al/organic interface. The above numerical simulations confirm the excitation and outcoupling of the broadband SPP modes in the dual-periodic-corrugated devices.

Figure 4 shows the angular-dependent electroluminescent (EL) spectra of the dual-periodic-corrugated WOLEDs. The additional peaks in the TM and TE polarized electroluminescence (EL) spectra and their shifts in wavelength as the angle varies can be clearly observed in Figure 4a and b. Compared with the polarized absorption spectra (Figure S3), their peak wavelengths are almost coincident, which demonstrates an efficient outcoupling of the photons from the trapped SPP modes, and improved light extraction is to be expected. The spectral shape differs between the absorption and EL emission spectra and a narrower bandwidth is observed in the EL spectra, because the fluorescence of the Bepp₂ and (bzq)₂Ir(dipba) may decide the bandwidth of the EL emission, while it has no influence on that of the absorption spectra. In the case of the nonpolarized EL emission as shown in Figure 4c, the WOLEDs exhibit stable EL spectra with variation of observation angle. The Commission

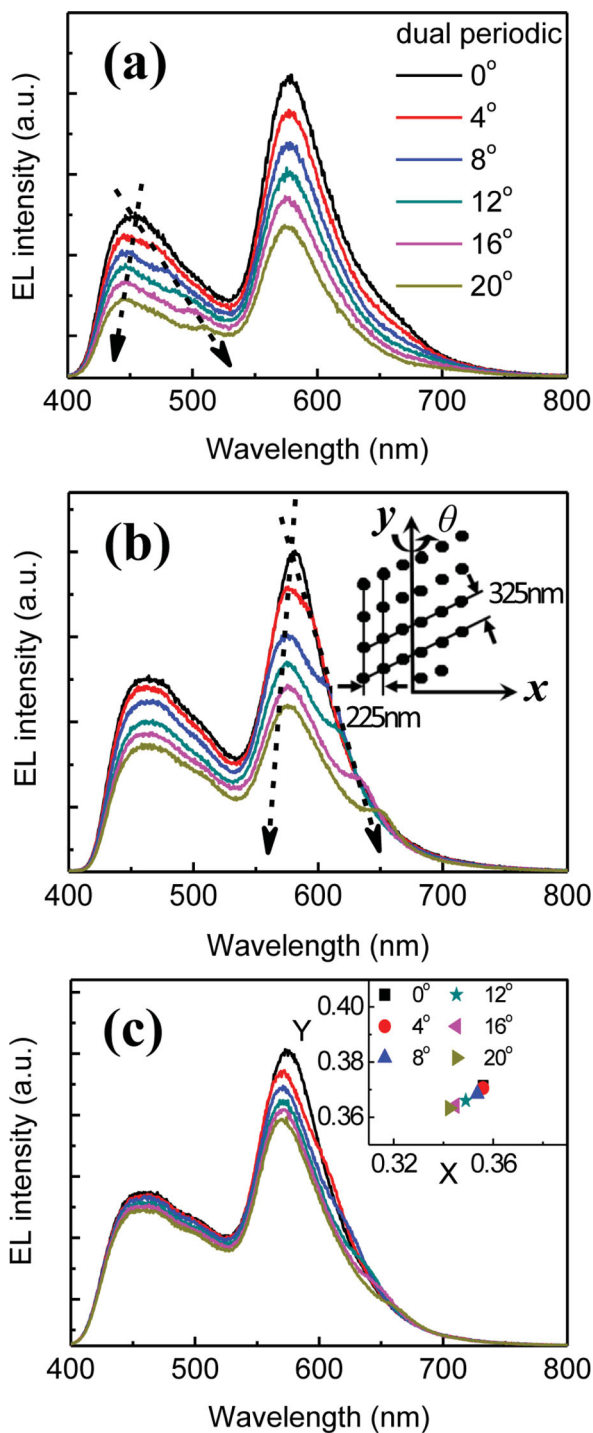


Figure 4. EL spectra at different observation angles of the dual-periodic-corrugated WOLEDs with a) TM, b) TE polarization and c) nonpolarization. The inset in (b) shows the orientation of the rotation axis. The inset in (c) shows the CIE coordinates of the 2D WOLEDs at various viewing angles.

International de l'Éclairage (CIE) coordinates show no apparent change with observation angle (inset in Figure 4c), which means that the dual-periodic corrugation has no negative

effect on the viewing characteristics of the WOLEDs, which is important for applications in both display and lighting. The broadband enhancement was verified by comparing the EL spectrum of the dual-periodic WOLEDs to those of the 1D corrugated and planar WOLEDs. As can be seen in Figure 5a, the 1D monoperoiodic WOLEDs with 225 and 325 nm periods show improvement in the blue and orange regions, respectively, compared to those of the planar WOLEDs. The dual-periodic corrugated WOLEDs show similar EL spectra to those of the planar devices, and the CIE coordinates are only slightly changed from (0.356, 0.373) for the planar WOLEDs to (0.358, 0.375) for the dual-periodic WOLEDs (Figure 5b). The simultaneous improvement in the blue and orange emission region for the 2D WOLEDs results in them having similar EL spectra and CIE coordinates to those of the planar devices. Therefore, the WOLEDs employing dual-periodic corrugation have the advantage that no special structural adjustment has to be made to redress the EL spectra after the dual-periodic corrugation is introduced into the device structure.

The effect of the broadband light extraction on the EL performance of the dual-periodic WOLEDs was examined by comparison with that of the 1D monoperoiodic corrugated and planar WOLEDs and is summarized in Figure 6. We also

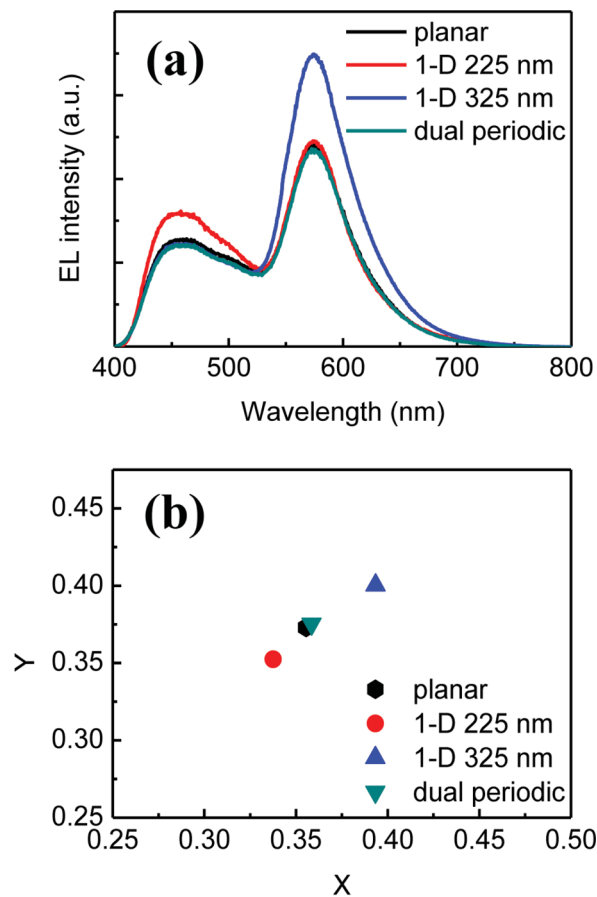


Figure 5. a) Normalized EL spectra and b) CIE coordinates of the corrugated and planar WOLEDs in the normal direction.

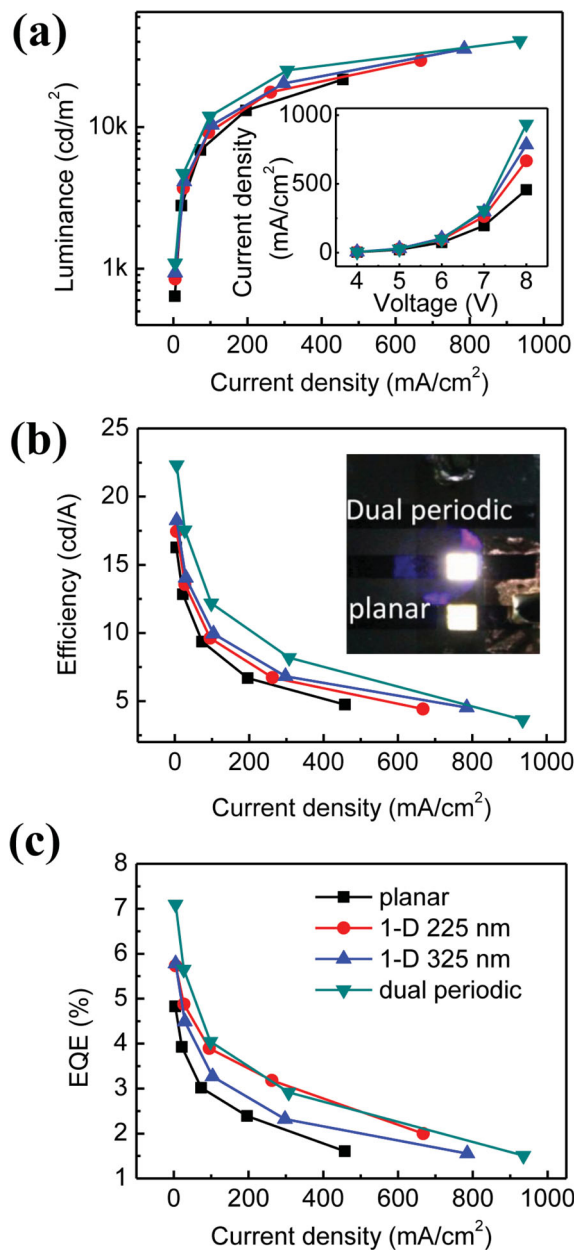


Figure 6. EL performance of the corrugated and planar WOLEDs. a) Current density–luminance, b) current density–efficiency, and c) current density–EQE characteristics of the corrugated and planar WOLEDs. The inset in (a) shows current density–voltage characteristics of the WOLEDs. The inset in (b) shows the photograph of the operating dual-periodic and planar WOLEDs on the same substrate and under the same driving voltage.

compared the EL performance of the planar WOLEDs based on ITO and Au thin film anodes (Figure S6). Despite the fact that the transparency of ITO is higher than that of Au thin film (Figure S7), the EL performance of the two WOLEDs is similar because of the use of the Au film as anode which permits the elimination of the power lost to WGs in ITO. The external quantum efficiency of WOLEDs was calculated by

using the EL spectra measured at different viewing angles, as described in the Experimental Section. The dual-periodic corrugated WOLEDs show obvious enhancement in both luminance and efficiency as expected. The maximum luminance increased from 21720 cd m⁻² for the planar device to 29510 cd m⁻² for the 1D 225 nm periodic device, 35587 cd m⁻² for the 1D 325 nm periodic device, and 40680 cd m⁻² for the dual-periodic device. The maximum current efficiency and external quantum efficiency (EQE) were improved from 16.27 cd A⁻¹ and 4.8 % for the planar device to 17.44 cd A⁻¹, 5.7 % for the 1D 225 nm periodic device, 18.25 cd A⁻¹ and 5.8 % for the 1D 325 nm periodic device, and 22.33 cd A⁻¹ and 7.1 % for the dual-periodic corrugated device. The 1D monophasic corrugated devices reveal 7.2 % (225 nm period) and 12.2 % (325 nm period) enhancement in current efficiency, and 18.8 % (225 nm period) and 20.8 % (325 nm period) enhancement in the EQE compared to those of the conventional planar device, along with a 37 % enhancement in the current efficiency and 48 % enhancement in EQE that results from integrating the dual-periodic corrugations. Combined with the above experimental and numerical results, the EL enhancement could be attributed to the broadband light extraction by the excitation and radiation of the broadband SPP modes at the cathode/organic interface induced by the dual-periodic corrugation.

In conclusion, dual-periodic corrugation has been introduced into WOLED metallic electrodes to realize broadband light extraction. The dual-periodic corrugation outcouples the trapped SPP modes in broadband by exciting the SPP resonance at two separate wavelengths, which are coincident with the blue and orange emission region of the two-color-based WOLEDs. A 37 % enhancement in current efficiency and 48 % enhancement in the external quantum efficiency compared to those of the conventional planar devices have been obtained. Besides the much improved efficiency, the dual-periodic-corrugated WOLEDs exhibit satisfying viewing characteristics. Therefore, employing the dual-periodic corrugation in WOLEDs has the potential to improve the commercial applications of the WOLEDs in both display and lighting.

Experimental Section

Preparation of the Dual-Periodic Corrugation: Holographic lithography was employed to fabricate the periodic corrugations. By adjusting the angle of the two laser beams, various periodic microstructures could be obtained. The photoresist (NOA63, Norland Products, Inc.) diluted in acetone at a concentration of 25 mg mL⁻¹ was spin-coated onto a pre-cleaned glass substrate at 6000 rpm speed for 20 s. The thickness of photoresist film was 100 nm. A continuous laser with 266 nm wavelength (Coherent Inc.) was used as light source for the lithography. The sample was exposed by two laser beams which were split from the UV laser with beam size of 6 mm in diameter. A 1D monophasic grating was obtained by exposing the photoresist to the interference fringes. For fabrication of the dual-periodic corrugation, the sample was exposed a second time after rotation by 60° with a different writing angle. The microstructure with different period and depth can be obtained by adjusting the writing angle and the exposure time. The morphologies of the microstructure were characterized by using atomic force microscopy (AFM, Dimension Icon, Bruker Corporation) in the tapping mode.

Numerical Simulation: The Drude model was chosen to deal with Al and Au. The refractive indices of other materials employed in WOLEDs were measured experimentally by ellipsometry for the FDTD calculation. Period boundary conditions and perfectly matched layers were set along the x y directions and z direction, respectively. The incident light was a modulated Gaussian pulse. The reflection, transmission, and absorption spectra could be obtained by Fourier transform.

WOLEDs Fabrication and Evaluation: Glass substrates coated with corrugated photoresist film were immediately loaded into a thermal evaporation chamber. A 15 nm semitransparent Au anode was deposited on the prepared substrates. A 5-nm MoO₃ anodic modification layer, 40-nm-thick hole-transporting layer of *N,N'*-diphenyl-*N,N'*-bis(1,1'-biphenyl)-4,4'-diamine (NPB), 20-nm-thick emitting layer of 2% wt bis(7,8-benzoquinolino) iridium(III) (*N,N'*-diisopropyl-benzamidine) ((bzoq)₂Ir(dipba)) doped into bis(2-(2-hydroxyphenyl)-pyridine)beryllium (Bepp₂), 45 nm electron-transporting layer of Bepp₂, and cathode of LiF (1 nm)/Al (80 nm) were evaporated sequentially at a base pressure of 5×10⁻⁴ Pa. The absorption spectra were measured by using a UV-Vis spectrophotometer (UV-2550, SHIMADZU). The angular-dependent electroluminescent spectra were measured by means of a fiber optic spectrometer. A slit was used to limit the angular acceptance to ~1°, and the OLEDs were placed on a rotation stage with grooves (one of the grooves for the 2D corrugation) parallel to the rotation axis. The current density–luminance characteristics of the devices were measured by using a Keithley 2400 programmable voltage–current source and Photo Research PR-655 spectrophotometer. The active area of the device was 2 × 2 mm². All of the measurements were conducted in air at room temperature.

External Quantum Efficiency Calculation: The EQE of WOLEDs (η_{ext}) was calculated by using Equation (1):^[20]

$$\eta_{\text{ext}} = \frac{\pi e}{K_m h c J} \int_0^{\frac{\pi}{2}} \left[L_v(\theta) \sin 2\theta \frac{\int \lambda P(\theta, \lambda) d\lambda}{\int P(\theta, \lambda) V(\lambda) d\lambda} \right] d\theta \quad (1)$$

where e is the quantity of the electron charge, K_m is a conversion constant based on the maximum sensitivity of the eye (683 lm W⁻¹), h is the Planck constant, c is the velocity of the light, J is current density, $P(\theta, \lambda)$ is the relative spectral power distribution of the device at viewing angle θ , $V(\lambda)$ is the normalized photopic spectral response function, and $L_v(\theta)$ is the spectral luminance at θ .

Supporting Information

Supporting Information is available from the Wiley Online Library or from the author.

Acknowledgements

The authors gratefully acknowledge support from 973 project (Grant No. 2011CB013005) and NSFC (Grant Nos. 61322402, 61177024, 91233123, and 61107024).

Received: May 24, 2013

Revised: August 3, 2013

Published online: September 24, 2013

- [1] Y. Sun, N. C. Giebink, H. Kanno, B. Ma, M. E. Thompson, S. R. Forrest, *Nature* **2006**, *440*, 908.
- [2] B. W. D'Andrade, S. R. Forrest, *Adv. Mater.* **2004**, *16*, 1585.
- [3] Y. G. Bi, J. Feng, Y. F. Li, Y. Jin, Y. F. Liu, Q. D. Chen, H. B. Sun, *Appl. Phys. Lett.* **2012**, *100*, 053304.
- [4] P. A. Hobson, S. Wedge, J. A. E. Wasey, I. Sage, W. L. Barnes, *Adv. Mater.* **2002**, *14*, 1393.
- [5] Y. Jin, J. Feng, X. L. Zhang, Y. G. Bi, Y. Bai, L. Chen, T. Lan, Y. F. Liu, Q. D. Chen, H. B. Sun, *Adv. Mater.* **2012**, *24*, 1187.
- [6] L. H. Smith, J. A. E. Wasey, I. D. W. Samuel, W. L. Barnes, *Adv. Funct. Mater.* **2005**, *15*, 1839.
- [7] Y. Bai, J. Feng, Y. F. Liu, J. F. Song, J. Simonen, Y. Jin, Q. D. Chen, J. Zi, H. B. Sun, *Org. Electron.* **2011**, *12*, 1927.
- [8] J. Feng, T. Okamoto, R. Naraoka, S. Kawata, *Appl. Phys. Lett.* **2008**, *93*, 051106.
- [9] X. L. Zhang, J. Feng, J. F. Song, X. B. Li, H. B. Sun, *Opt. Lett.* **2011**, *36*, 3915.
- [10] W. H. Koo, S. M. Jeong, F. Araoka, K. Ishikawa, S. Nishimura, T. Toyooka, H. Takezoe, *Nat. Photonics*, **2010**, *4*, 222.
- [11] W. H. Koo, W. Youn, P. Zhu, X. Li, N. Tansu, F. So, *Adv. Funct. Mater.* **2012**, *22*, 3454.
- [12] M. G. Helander, Z. B. Wang, M. T. Greiner, Z. Liu, J. Qiu, Z. Lu, *Adv. Mater.* **2010**, *22*, 2037.
- [13] X. Li, W. C. H. Choy, L. Huo, F. Xie, W. E. I. Sha, B. Ding, X. Guo, Y. Li, J. You, Y. Yang, *Adv. Mater.* **2012**, *24*, 3046.
- [14] T. Peng, Y. Yang, H. Bi, Y. Liu, Z. Hou, Y. Wang, *J. Mater. Chem.* **2011**, *21*, 3551.
- [15] R. Wang, D. Liu, H. Ren, T. Zhang, H. Yin, G. Liu, J. Li, *Adv. Mater.* **2011**, *23*, 2823.
- [16] D. M. Koller, A. Hohenau, H. Ditlbacher, N. Galler, F. Reil, F. R. Aussenegg, A. Leitner, E. J. W. List, J. R. Krenn, *Nat. Photonics*, **2008**, *2*, 684.
- [17] W. L. Barnes, A. Dereux, T. W. Ebbesen, *Nature*, **2003**, *424*, 824.
- [18] W. C. Liu, D. P. Tsai, *Phys. Rev. B* **2002**, *65*, 155423.
- [19] C. J. Yates, I. D. Samuel, P. L. Burn, S. Wedge, W. L. Barnes, *Appl. Phys. Lett.* **2006**, *88*, 161105.
- [20] F. Y. Ma, J. P. Su, M. T. Guo, Q. X. Gong, Z. Y. Duan, J. Yang, Y. L. Du, B. Yuan, X. Y. Liu *Opt. Commun.* **2012**, *285*, 3100.